Original Research Paper

Restructuring capability of non-fractal aggregate in simple shear flow

Uyen Tu Lieu *, Shusaku Harada

Division of Sustainable Resources Engineering, Faculty of Engineering, Hokkaido University, N13W8, Sapporo 060-8628, Japan

ABSTRACT

A unique pattern interpreting the restructuring of non-fractal aggregate is established. The restructuring of an aggregate from initial structure toward a stable structure is well presented by a linear relation between the saturation degree of particle connection, and the inversed strength of aggregate. The dynamics of restructuring for different initial configuration of aggregate, from very loose to dense, in various simple shear flow condition is numerically performed. The temporal change in properties of aggregate is analyzed in terms of coordination number and volume fraction. The simulation employs Stokesian dynamics for the estimation of many-particle hydrodynamic interaction while the particle–particle interaction is calculated by van der Waals potential. Simulation results show that the aggregate restructures and exists in a stable state corresponding to the shear flow condition. The transition among the stable aggregates somewhat expresses reversible behavior. Especially in weak flow, the aggregate gradually reaches its limit structure whose properties such as coordination number and volume fraction are typically determined. Such limit aggregate plays an important role for predicting the restructuring of any non-fractal aggregate in any fluid condition. Moreover, the penetration effect of fluid flow on aggregate is discussed by means of porous sphere model.

© 2016 The Society of Powder Technology Japan. Published by Elsevier B.V. and The Society of Powder Technology Japan. All rights reserved.

1. Introduction

The behavior of colloidal aggregate in fluid flow is fundamentally important for the prediction and control of dispersion of particles. In general, the behavior of aggregate in flow field, such as rigid-like motion, restructuring and breakup, depends on the hydrodynamic stress acting on the aggregate, and the strength of aggregate itself [1–5]. The task of determining such hydrodynamic stress and strength of aggregate is very complicated since the colloidal aggregate has a wide variety of structure which greatly affects those properties. The restructuring of aggregate, where the primary particles of the aggregate are relatively in motion but still attach together, can be considered as an intermediate stage between the rigid-like motion and breakup. While the breakup of aggregate is well established by extensive studies [1,2,4–9], the restructuring has not been properly understood. The restructuring of aggregate has significant impact on the breakup and aggregation of aggregate [10,11] because it possibly occurs either before [4,8] or after the breakup event [6,9]. As a result, the structure of aggregate and, consequently, the rheological properties of the colloidal suspension are completely affected.

The behavior of aggregate in simple shear flow has attracted a lot of interest due to its ubiquity in engineering fields. Fractal dimension, which can be interpreted as a space-filling property, is often used to characterize the structure of particle aggregates. In non-sheared system, the aggregate often has ramified structures whose fractal dimension is low. In sheared system, the aggregate appears more compact and is apt to exist in the form of high fractal dimension, which is demonstrated by experiment [1], simulation [6,9,12], and analytical model [13]. One of the possible reasons is that the restructuring of the aggregate has occurred, the branches of the aggregate bends and reconnects, leading to a more compact structure [4,5,14]. Furthermore, the breakup of the high fractal dimension aggregate behaves diversely whereas that of the low fractal dimension aggregate is predictable [4,15]. Explanation for the former can be analyzed from two perspectives. From the static point of view, the complex connectivity inside the high fractal aggregate influences the way of distribution and propagation of force, therefore the resulting stress differs within parts of the aggregate [15,16]. From the dynamic point of view, the restructuring of aggregate occurs, leads to significant change in aggregate's structure compared to its initial configuration, and eventually determines the way that the aggregate breaks [4,17,18]. Therefore, understanding the restructuring behavior of high fractal dimension aggregate contributes important information for kinetics of

* Corresponding author. Tel./fax: +81 11 706 6311.
  E-mail address: uyen@trans-er.eng.hokudai.ac.jp (U.T. Lieu).

aggregation model and breakup model. The aggregates at upper limit of fractal dimension, $d_f = 2.0$ for two-dimensional or $d_f = 3.0$ for three-dimensional aggregate, are dense and radial-density independent structures [16]. In the scope of this study, we define such aggregate as non-fractal aggregate to emphasize the difference of its structure compared to the fractal and ramified aggregate. Experimental study for two-dimensional non-fractal aggregate shows that there is a significant change in the internal structure of aggregate: under shear flow, the particles of the aggregate rearrange into a more ordered structure [19]. For three-dimensional aggregate [1], the change of internal structure of aggregate is unknown due to lack of proper observing devices. We have conducted numerical simulation to study about the restructuring behavior of non-fractal aggregate in the previous work [20]. We have found that in simple shear flow, the non-fractal aggregate restructures via change in internal connectivity so that a more stable structure is obtained. Such stable structure has similar appearance but notable difference in internal connectivity compared to the initial structure. A kinetic model represents change in coordination number of aggregate is proposed.

The content of this article shows succeeding output of our previous study [20]. The previous article focuses on the existence of stable aggregate during the restructuring, and the dependence of the internal connectivity of aggregate on the condition of fluid flow as well as the initial aggregate. In this article, we attempt to establish a comprehensive approach to predict the corresponding structure of a given aggregate in simple shear flow by considering the physical interpretation of the restructuring in terms of the capacity of making particle connection and the strength of aggregate. In detail, investigations for the uniqueness of stable aggregate, the limit of restructuring, the governing properties that decide the structure of aggregate, and the role of hydrodynamic stress, are carried out. The dynamics of restructuring behavior of non-fractal aggregates before breakup in simple shear flow is performed by Lagrangian simulation approach. The many-body hydrodynamic interaction among the identical particles composing the aggregate is estimated by Stokesian dynamics. The restructuring of non-fractal aggregate with different initial configuration is examined under various fluid shear flow conditions.

2. Simulation method

The simulation method is almost similar to our previous study [20]. For convenience, we emphasize the concept, governing equations and simulation conditions of the study. The basis of our simulation method for the hydrodynamic interaction of multiple particles in fluid flow is Stokesian dynamics [21,22]. The content of the lengthy and complicated Stokesian dynamics can be found in the work of Durlofsky et al. [22] and the references therein. The FTS version of Stokesian dynamics is used to study the motion of particles in an imposed flow. In summary, when the particle is in relative motion to the fluid flow, the particle exerts force $\boldsymbol{F}_H$ and torque $\boldsymbol{T}_H$ on fluid. In opposite, fluid exerts on particle the hydrodynamic force $-\boldsymbol{F}_H$, torque $-\boldsymbol{T}_H$, and stresslet S. For a particle with hydrodynamic interaction $-\boldsymbol{F}_H, -\boldsymbol{T}_H$ and non-hydrodynamic interaction $\boldsymbol{F}, \boldsymbol{T}$, the neglect of particle inertia leads to $\boldsymbol{F}_H \approx \boldsymbol{F}$ and $\boldsymbol{T}_H \approx \boldsymbol{T}$. Finally, for a finite number of particles in fluid flow, the relation between the force exerting on particles and the relative motion of particles to the fluid flow is shown as following

$$\begin{pmatrix} \boldsymbol{F} \\ \boldsymbol{T} \\ \boldsymbol{S} \end{pmatrix} = \boldsymbol{M}^{-1} \cdot \begin{pmatrix} \boldsymbol{U} - \boldsymbol{u}^\infty \\ \boldsymbol{\Omega} - \boldsymbol{\Omega}^\infty \\ -\boldsymbol{E}^\infty \end{pmatrix}, \boldsymbol{M}^{-1} = \begin{pmatrix} \boldsymbol{R}_{FU} & \boldsymbol{R}_{F\Omega} & \boldsymbol{R}_{FE} \\ \boldsymbol{R}_{TU} & \boldsymbol{R}_{T\Omega} & \boldsymbol{R}_{TE} \\ \boldsymbol{R}_{SU} & \boldsymbol{R}_{S\Omega} & \boldsymbol{R}_{SE} \end{pmatrix} \quad (1)$$

where $\boldsymbol{U}, \boldsymbol{\Omega}$ is the particle velocity and rotational velocity; $\boldsymbol{u}^\infty, \boldsymbol{\Omega}^\infty, \boldsymbol{E}^\infty$ the velocity, rotational velocity and rate of strain tensor

of the undisturbed flow; $\boldsymbol{R}_{FU}, \boldsymbol{R}_{TU}$, etc. the components of the resistance matrix which are determined from the mobility matrix $\boldsymbol{M}$ and dependent only on the position of the particles. The calculation method of the mobility matrix $\boldsymbol{M}$ can be found in Durlofsky et al. [22]. According to Eq. (1), the translational and rotational velocity of particles is calculated as below

$$\begin{pmatrix} \boldsymbol{U} \\ \boldsymbol{\Omega} \end{pmatrix} = \begin{pmatrix} \boldsymbol{u}^\infty \\ \boldsymbol{\Omega}^\infty \end{pmatrix} + \begin{pmatrix} \overline{\boldsymbol{R}}_{FU} & \overline{\boldsymbol{R}}_{F\Omega} \\ \overline{\boldsymbol{R}}_{TU} & \overline{\boldsymbol{R}}_{T\Omega} \end{pmatrix}^{-1} \cdot \left[\begin{pmatrix} \boldsymbol{F} \\ \boldsymbol{T} \end{pmatrix} + \begin{pmatrix} \overline{\boldsymbol{R}}_{FE} \\ \overline{\boldsymbol{R}}_{TE} \end{pmatrix} : \boldsymbol{E}^\infty \right] \quad (2)$$

where $\overline{\boldsymbol{R}}_{FU}, \overline{\boldsymbol{R}}_{F\Omega}$, etc. are the components of the grand resistance matrix $\overline{\boldsymbol{R}}$ in which the lubrication correction is included by the following form

$$\overline{\boldsymbol{R}} = \boldsymbol{M}^{-1} - \boldsymbol{M}_{2B}^{-1} + \boldsymbol{R}_{2B} \quad (3)$$

where $\boldsymbol{M}_{2B}$ is the two-body mobility matrix calculated in a similar way with $\boldsymbol{M}$, $\boldsymbol{R}_{2B}$ the two-body resistance matrix [22–24]. The dynamic behavior of all particles is performed by numerical integration of Eq. (2) while the matrices are continuously updated with each time step.

The behavior of an isolated aggregate is investigated in simple shear flow characterized by shear rate $\dot{\gamma}$. The undisturbed flow $\boldsymbol{u}^\infty = (\dot{\gamma}y, 0, 0)^T$ in Cartesian coordinates, which is viably used in Eq. (2), is described as

$$\boldsymbol{u}^\infty(\boldsymbol{r}) = \boldsymbol{\Omega}^\infty \times \boldsymbol{r} + \boldsymbol{E}^\infty \cdot \boldsymbol{r} \quad (4)$$

$$\boldsymbol{\Omega}^\infty = -\frac{\dot{\gamma}}{2} \begin{pmatrix} 0 \\ 0 \\ 1 \end{pmatrix}, \quad \boldsymbol{E}^\infty = \frac{\dot{\gamma}}{2} \begin{pmatrix} 0 & 1 & 0 \\ 1 & 0 & 0 \\ 0 & 0 & 0 \end{pmatrix} \quad (5)$$

The simulation condition is similar to our previous study [20]; the summary can be found in Table 1. The interaction between the hard-sphere particles is estimated by retarded van der Waals potential based on Hamaker geometrical factor and Lifshitz theory. The complicated formulae for the renowned potential are completely given in the relevant articles [25,26]. Additionally, when the surface distance of particles is less than a cutoff distance of 1 nm, the attractive force is simply set zero since the other complex phenomena at molecular scale may be dominant and should be taken into account [27]. The overlap of particles does not occur due to the lubrication correction and suitably small time-step. Recently, researches on the behavior of aggregate sometimes involve more complicated interparticle interaction, e.g. tangential force, due to its significant effect on the restructuring fractal aggregate [5,6,14]. In particular, it is reported that the branches of the fractal aggregate is more invulnerable to bending moment [5,6,28]. However, a systematic understanding on such tangential force has not been well established yet, leading to difficulties and uncertainties in constructing models. Our simulation with the prescribed force in this study is simple but able to represent an example of particle aggregates with central force, and the scope of our study is to examine the effect of hydrodynamics of many-body rather than the effect of interparticle interaction on the aggregate.

Table 1
Basic simulation conditions.

Parameter	Value
Number of particle of aggregate	$N = 100$
Particle radius	$a = 325$ nm
Particle density	$\rho_p = 1056$ kg/m^3
Fluid density	$\rho_f = 790$ kg/m^3
Fluid viscosity	$\mu = 1.2 \times 10^{-3}$ Pa s
Non-retarded Hamaker constant (for the condition of this study)	$A_H = 9.68 \times 10^{-21}$ J
Cut-off distance	$\delta = 1$ nm

Due to these reasons, we do not consider tangential force in the simulation. We have found that although the force model in our study is simple, some properties expressing the dynamic behavior of aggregate in fluid flow is reasonably comparable with experiment results [3,18] and simulation results [6,29] where more complex force model is applied. About the simulation condition, the effect of fluid inertia, particle inertia and Brownian motion of particle is negligible because of small Reynolds number, Stokes number and large Péclet number. Further discussion on the assumptions, calculation conditions and validation of the simulation can be found in the articles [4,17].

Basically, the same non-fractal aggregate as previous paper is investigated [20]. The initial appearance (at $\dot{\gamma}\,t = 0$) of some aggregate is given in Fig. 1a. The non-fractal aggregate is created by utilizing the particle-cluster aggregation model while applying centripetal force to a given number of particles randomly distributed [30]. This simulation procedure for assembling the aggregate is independently carried out before the aggregate is subjected to fluid flow, meaning that from the onset of simple shear flow, the force model for interaction between particles is the retarded van der Waals and the hydrodynamic interaction. In order to identify the cause of the restructuring, we have conducted the simulation for the aggregate with the used interparticle interaction in zero shear condition. The aggregate remains almost the same state after a long time, suggesting that the restructuring of the aggregate is triggered by the motion of fluid flow. The average coordination number is used to evaluate the internal connectivity of the aggregate during its restructuring. The coordination number for an identified particle is defined as the number of its surrounding particles within a designated separation of particle surface which is chosen to be 2 nm. The value of coordination number is verified not dramatically affected if the designated separation varies with a few nanometers. The initial configuration of the aggregate ranges from a very loose structure, whose coordination number is low at $k_0 = 2.00$, to intermediate ones with $k_0 = 3.02$, 4.20 and 5.04, then to a very dense structure, $k_0 = 5.54$ [20]. Regarding the sensitiveness of the restructuring result to the number of aggregate, we have created five independent aggregates for a given initial configuration and performed the simulation at some conditions related to initial configuration and fluid shear flow. The properties of the aggregate at the stable state are determined. A standard deviation within 2% of the mean is found out. In the previous studies [17,20] the coordination number is an important parameter because it directly represents the internal structure of the aggregate. In this paper, the coordination number is revealed inadequate to understand the restructuring nature of the aggregate. Therefore, we additionally determine the effective volume fraction of the aggregate, and subsequently introduce the other properties such as the saturation degree of connectivity, and strength of aggregate. The details will be given in the next section. Aside from the aggregates
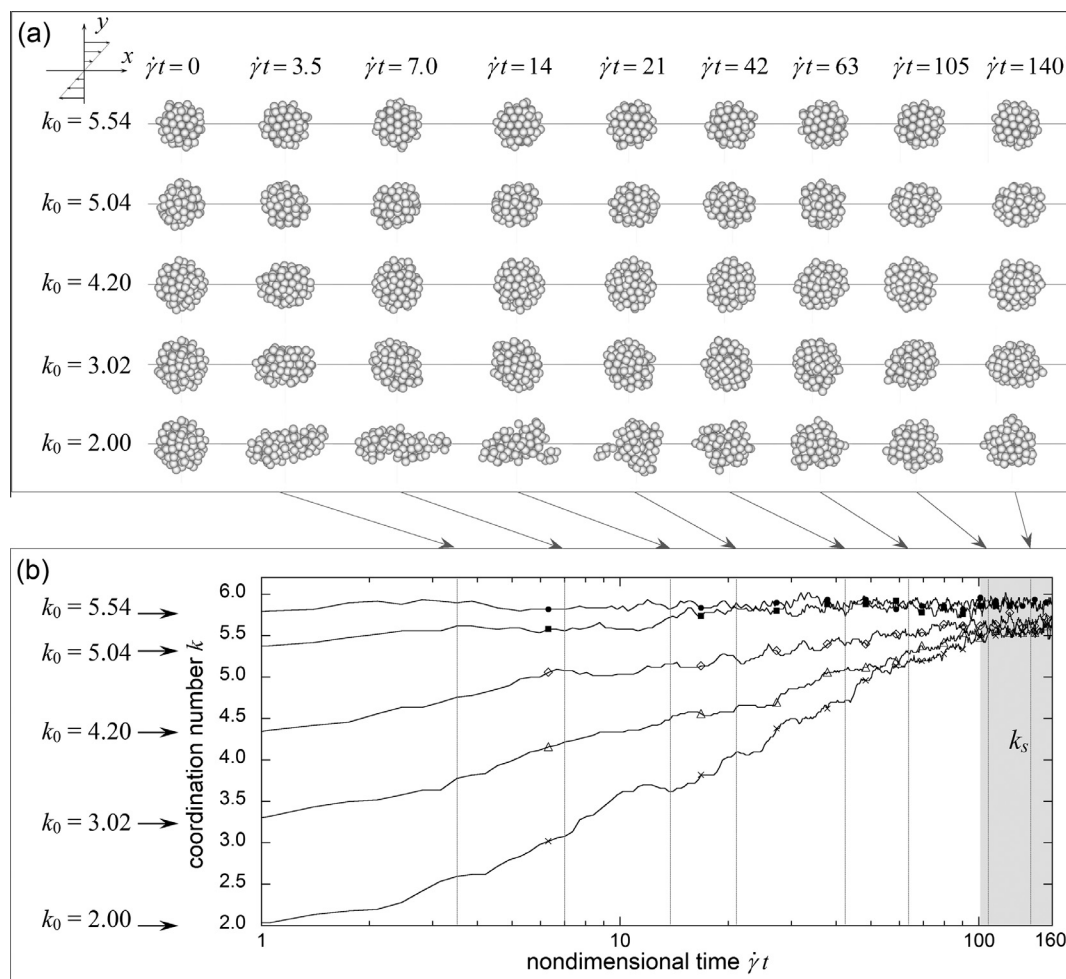

Fig. 1. Temporal change in (a) shape and (b) coordination number of various aggregates in fluid shear stress condition $\mu\dot{\gamma} = 26.9$ Pa. The arrow is to indicate the position of $\dot{\gamma}\,t$ in (b). Some data are obtained from [20].

mentioned earlier, new aggregates are prepared in this study. They are non-fractal aggregates whose k_0 = 2.50, 3.98, 4.80, and a fractal aggregate whose fractal dimension and initial coordination number are d_f = 1.8 and k_0 = 2.00, respectively.

3. Results and discussion

3.1. Change in coordination number

As mentioned in the introduction, the previous work has found out that in simple shear flow, the non-fractal aggregate restructures into another configuration by changes in either outer shape or internal connectivity [20]. Fig. 1 shows the temporal change in such two properties for five non-fractal aggregates at the same fluid shear stress condition $\mu\dot{\gamma}$ = 26.9 Pa. Part of data are extracted from our previous study [20]. In terms of deformation of its shape, Fig. 1a shows that the aggregate instantly deforms from sphere to ellipsoid at the onset of shear flow at $\mu\dot{\gamma}$ = 26.9 Pa; as time continues, the ellipsoidal aggregate gradually turns into spherical one while rotating around the vorticity axis. This behavior occurs when the initial structure of the aggregate is rather loose (k_0 = 2.00, 3.02, 4.20): the more loose aggregate exhibits more obvious deformation. In the case that the aggregate is dense (k_0 = 5.04, 5.54), the aggregate rotates and shows almost no visible change in its shape. In parallel, Fig. 1b, conducted at the simulation condition similar to Fig. 1a, expresses the coordination number k of aggregate proceeding with nondimensional time $\dot{\gamma}\,t$ [20]. Whether the deformation of shape is significant or not, changes in coordination number for all aggregates are observed until leveled-off values are reached, which are defined as the stable coordination number k_s as shown in the gray area. Since such stable structure is important, the dependence of stable coordination number k_s on the fluid shear stress $\mu\dot{\gamma}$ for all aggregates is examined and displayed in Fig. 2. In this figure, we only consider the case where the restructuring of aggregate is not significantly influenced by breakup. Discussion on the result can be found in our previous work [20]. Here, the important information for this work is that (i) the stable coordination number of aggregate k_s is significantly different from the initial one k_0, (ii) at the same $\mu\dot{\gamma}$ condition, little difference of k_s is observed among aggregates, and (iii) k_s linearly decreases with fluid shear stress $\mu\dot{\gamma}$ when $\mu\dot{\gamma}$ is relatively high; otherwise, as the flow is weak below a certain value $\mu\dot{\gamma}^*$, the stable coordination number k_s is a constant independent of fluid flow. We define the stable aggregate in weak flow as limit aggregate with k_{max}. The existence of k_{max} implies the limit of the restructuring for

non-fractal aggregate, i.e., the simple shear flow is capable of compacting the non-fractal aggregate until a limit state is reached. Slightly difference in the value of k_{max} is observed for the loose aggregate group (k_0 = 2.00, 3.02, 4.20) whose $k_{max} \approx 5.95$ and the dense group (k_0 = 5.04, 5.54) whose $k_{max} \approx 6.10$. Such slight difference of k_{max} makes it hard to conclude whether it is caused by either the particles at the outer layer or the inherent structure of aggregate. However, the gaps of k_s between the aggregates suggest little dependence on the initial aggregate.

In order to find the relation of the initial aggregate and limit aggregate (i.e. the stable structure of aggregate obtained in weak flow), a reversed simulation is carried out. Fig. 3 shows how the initial aggregate (for the case k_0 = 2.00, 5.54) and its limit aggregate affect the stable structure at $\mu\dot{\gamma}$ = 26.9 Pa. As given in the figure, the initial aggregate k_0 at a shear rate of $\mu\dot{\gamma}$ = 26.9 Pa restructures to its stable state. At the same time, the aggregate with k_0 gradually obtains the limit structure k_{max} in weak flow $\mu\dot{\gamma}$ = 12.0 Pa, then such corresponding k_{max} aggregate is subjected to a stronger flow condition $\mu\dot{\gamma}$ = 26.9 Pa, and the new stable structure is observed. It reveals that such a new stable coordination number is similar to the value at which the initial aggregate k_0 directly achieves in strong fluid flow condition $\mu\dot{\gamma}$ = 26.9 Pa. This behavior is met for both the very loose aggregate k_0 = 2.00 and the very dense aggregate k_0 = 5.54. The results indicate that the stable aggregates corresponding to given conditions of simple shear flow are somewhat reversible. Perhaps the limit aggregate obtained at weak flow can act as a "standard" for the restructuring. Studying on the properties of limit aggregate can provide important information for the prediction of aggregate behavior.

As mentioned earlier, the small difference of k_{max} values in Fig. 2 seems inadequate to interpret the limit structure. Therefore, we investigate another property of the aggregate: volume fraction ϕ. The volume fraction of aggregate is defined as the ratio of volume of all particles to the volume occupied by aggregate, which is considered as an ellipsoid having the same principal moment of inertia [31]. Readers may refer to Appendix A.1 for the detailed calculation. Fig. 4 shows the temporal change in coordination number and volume fraction for the aggregate k_0 = 3.02 at various shear conditions. The inset shows the data for weak flow $\mu\dot{\gamma}$ = 12.0 Pa. The horizontal line indicates the coordination number k_{max} and volume fraction ϕ_{max} of the limit aggregate at $\mu\dot{\gamma}$ = 12.0 Pa. The coordination number and volume fraction of aggregate are
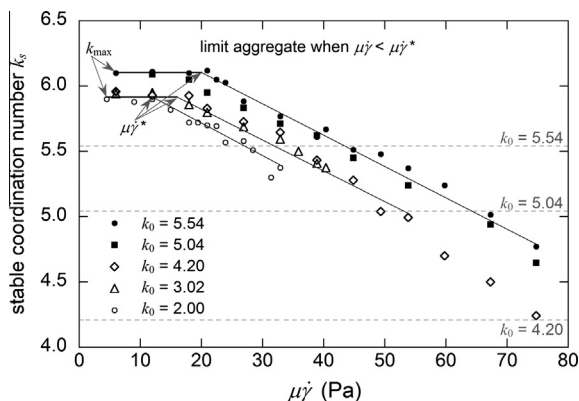

Fig. 2. Stable coordination number k_s of aggregates at various shear flow conditions $\mu\dot{\gamma}$. Some data are extracted from [20]. The black lines along the points are to guide the eye. The dash-horizontal lines shows the initial coordination number of aggregate before subjected to flow $\mu\dot{\gamma}$.
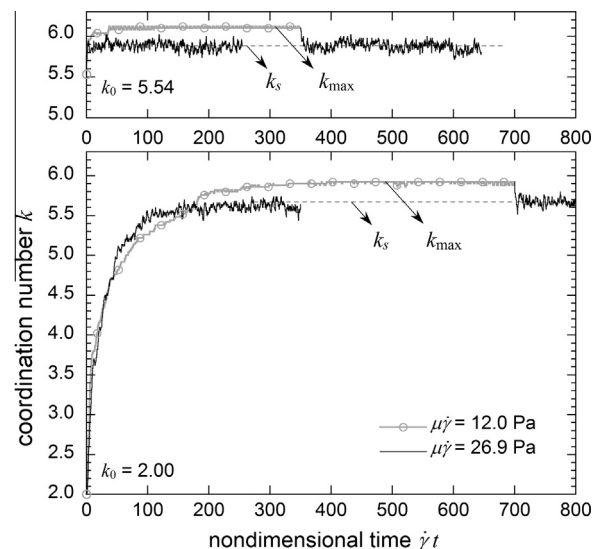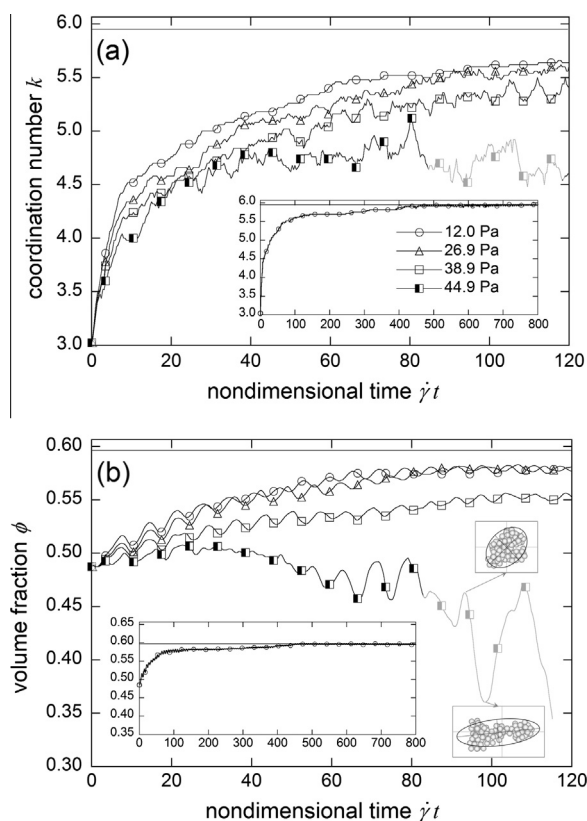

Fig. 3. Coordination number profile for aggregate at initial structure k_0 and limit structure k_{max} at the same shear flow condition $\mu\dot{\gamma}$ = 26.9 Pa.

Fig. 4. Change in (a) coordination number k and (b) volume fraction ϕ at various shear flow conditions for the aggregate with $k_0 = 3.02$. The horizontal line shows the value of k_{max} and ϕ_{max} for this aggregate. The blurred profile shows the irregular change of aggregate toward breakup. Legend in (a) and (b) has the same meaning.

Table 2
Typical properties of limit aggregate obtain at weak flow condition $\mu\dot{\gamma}$ = 12.0 Pa.

k_0	ϕ_0	k_{max}	ϕ_{max}
2.00, fractal	0.054	5.90	0.500
2.00	0.371	5.92	0.516
2.50	0.438	5.94	0.570
3.02	0.488	5.96	0.596
3.98	0.534	5.90	0.590
4.20	0.559	5.92	0.602
4.80	0.618	5.95	0.628
5.04	0.654	6.09	0.658
5.54	0.665	6.10	0.666

by ϕ_{max} rather than k_{max}. The reason explaining such a situation that the aggregate has quite similar coordination number but different volume fraction possibly originates from the arrangement of the particles. Although the coordination number describes the average number of connection of particles, the distribution of these connections cannot be expressed by coordination number but partly by the volume fraction. The other issue is the dependence of ϕ_{max} on the initial configuration of aggregate. As can be seen in Table 2, aggregate of smaller ϕ_0 results in smaller ϕ_{max}. Moreover, by conducting similar simulation for the other non-fractal aggregates, we have found that the ϕ_{max} is somewhat typical value depending on the initial one. Such typical ϕ_{max} is approximately 0.52 for initial aggregate of very loose structure (even including the fractal aggregate with fractal dimension $d_f = 1.8$), 0.59 for moderate loose one. The dense aggregate does not vary ϕ_{max} so much compared to ϕ_0. Limit structure of the fractal aggregate is in agreement with Seto et al. [14]. In their study, the fractal aggregate restructures to a more compact spherical or rod structure whose volume fraction is about 0.48–0.54 [14], similar to $\phi_{max} \approx 0.50$ in our study. In conclusion, the properties of the limit aggregate, k_{max} and ϕ_{max} become available for the investigated conditions of this study. The dependence of ϕ_{max} on ϕ_0 is unclear. It may relate to the mobility of the particle during the restructuring of aggregate. Interestingly, we find out that the compaction of the limit aggregate is quite similar to the jammed packing of identical hard spheres in two aspects: (i) the range of ϕ_{max} in our study $\phi_{max} \approx 0.50$–0.66 while the volume fraction of jammed-packing is in the range of 0.52–0.74, and (ii) how the initial volume fraction affects final one [32]. Another notable point on the restructuring of the three-dimensional aggregate in our study is that, the restructuring in weak flow for a loose aggregate, whose initial volume fraction is less than the random close packing or initial coordination number is less than about 6, results in more compact structure but does not exceed the random close packing limit. Meanwhile, the restructuring of two-dimensional aggregate possibly leads to a more compact and more order structure [19].

3.2. Kinetic behavior of the restructuring

The temporal coordination number and volume fraction of aggregate are dependent on the shear flow condition (see Figs. 1b and 4). Our attempt is to find a physical relation of these properties by introducing two parameters. Firstly, we consider the ratio of the number of unlinked particle to linked particle, defined as $(k_{max} - k)/k$, where k_{max} are taken from Table 2. This ratio roughly indicates the saturation degree of the internal connectivity, or the capability of forming connection among particles. As the non-negative value $(k_{max} - k)/k$ approaches zero, the particles are more saturated and less capable of rearranging their relative position to make more connection. Secondly, we determine the value $1/(k\phi)$, representing the inversed strength of aggregate according to Rumpf's theory [33]:

determined when the aggregate still keeps a spherical or ellipsoidal shape. When the shape of aggregate is irregular and toward breakup, the fitting ellipsoid is no longer suitable to describe the occupied space of the aggregate. Illustration of the irregular aggregate and its equivalent ellipsoid in xy plane in Fig. 4 demonstrates the inapplicability of fitting ellipsoid method. Therefore, we do not continue the calculation for such cases. The figure shows that the volume fraction profile is smooth, whereas the coordination number one is sharply fluctuated. This is because the later is directly determined from each particle of the aggregate, which reflects the connectivity at a local scale. On the other hand, fitting the aggregate by the equivalent ellipsoid involves the global characteristic. Consequently, the temporal change in volume fraction is more gradual and less abrupt than that of coordination number. As can be seen in Fig. 4, during the restructuring of aggregate, the behavior of volume fraction is quite similar to coordination number, such as the change to stable value, and the dependence on fluid flow. The result suggests that there is a correlation between the coordination number and the volume fraction during the restructuring of the non-fractal aggregates. However, this correlation, as shown in Fig. 4, seems complicated because there are many affecting factors such as the initial configuration of the aggregate and the fluid shear stress. Moreover, we find that the limit structure of aggregate in weak flow also has highest volume fraction ϕ_{max}. Table 2 gives the properties of several aggregates at the weak flow condition of $\mu\dot{\gamma}$ = 12.0 Pa. The data shows that for the limit structure of the aggregate, the difference of volume fraction ϕ_{max} ($\phi_{max} \approx 0.50$–0.66) is more significant than that of coordination number k_{max} ($k_{max} \approx 5.90$–6.10). In other words, the effect of initial aggregate on limit aggregate is clearly expresses

$$\sigma_{Rumpf} = \frac{9F}{8\pi d^2} k\phi \propto k\phi \qquad (6)$$

where σ_{Rumpf} is the tensile strength of aggregate, F the maximal attractive force between two particle, d the diameter of particle. The value of the proportional factor $9F/(8\pi d^2)$ is approximately $9F/(8\pi d^2) = \sigma_0 \approx 220\ Pa$ regarding the conditions of this study. Since k and ϕ change during the restructuring of aggregate, $(k_{max} - k)/k$ and $1/(k\phi)$ are also functions of nondimensional time. Then instead of observing the temporal change in k and ϕ, and the dependence on fluid flow field $\mu\dot{\gamma}$, we calculate the saturation degree of connectivity $(k_{max} - k)/k$ and the inversed strength of aggregate $1/(k\phi)$ during the restructuring of aggregate. Fig. 5 shows the relation of $(k_{max} - k)/k$ and $1/(k\phi)$ during the restructuring of aggregate at various shear stress $\mu\dot{\gamma}$ for different initial aggregate from loose ($k_0 = 2.00$) to dense ($k_0 = 5.54$). In detail, Fig. 5b presents the result for aggregate $k_0 = 3.02$. Such data in Fig. 5b are calculated from the data in Fig. 4. While Fig. 4 shows that the dependence of k and ϕ on nondimensional time $\dot{\gamma}\ t$ and fluid shear stress $\mu\dot{\gamma}$ is complicated and unpredictable, Fig. 5b reveals a simple characteristic of restructuring process from the initial structure toward the stable one in terms of $(k_{max} - k)/k$ and $1/(k\phi)$: a linear trend. Such a linear trend is observed for all investigated aggregates in the study (Fig. 5a–e). For the case of loose aggregate ($k_0 = 2.00, 3.02, 4.20$), Fig. 5a–c indicates that there is a shift from the initial value toward smaller ones when the restructuring of aggregate occurs, i.e. the aggregate gradually develops more internal connection and increases its strength until a stable structure is reached. The position of stable point depends on the flow field and is not clearly shown. The discussion about the stable states will be examined later. As for the very dense aggregate ($k_0 = 5.04,\ 5.54$), Fig. 5d and e shows that aside from the aforementioned behavior,

the aggregate is able to shift from initial position outward the origin of the graph when the flow is strong enough. It means that the dense aggregate can becomes loose, but still maintain a specific relation between the internal connection and strength of aggregate. Generally, during the restructuring of given aggregate, the parameter $(k_{max} - k)/k$ and $1/(k\phi)$ are linearly related regardless the condition of shear flow. It is implied that if the limit structure (i.e. the aggregate in weak flow, whose position in Fig. 5 is the intersection with horizontal axis) of a given aggregate is known, one can predict the relation of saturation degree and inversed strength of aggregate.

About the restructuring of a given aggregate characterized by initial coordination number k_0, it has been previously shown in Fig. 2 that the aggregate restructure to a stable state k_s corresponding to the applied fluid flow condition $\mu\dot{\gamma}$; especially in low shear rate region, k_s reaches its maximal value defined as k_{max}. Fig. 5, which relates the saturation degree of connection among particles $(k_{max} - k)/k$ to the inversed strength of aggregate $1/(k\phi)$, and expresses how these properties change when the aggregate restructures from the initial configuration to the stable one, is still insufficient to provide the corresponding stable structure for fluid shear stress $\mu\dot{\gamma}$. It is noted that in Fig. 5, the represented position of stable structure, whose coordinates for horizontal axis and vertical axis are $1/(k_s\phi_s)$ and $(k_{max} - k_s)/k_s$, respectively, still belongs to the linear trend. Now we analyze the properties of aggregates at stable states corresponding to flow conditions. At each applied shear stress $\mu\dot{\gamma}$, the saturation degree of stable aggregate defined as the ratio of unlinked particle to linked particle $(k_{max} - k_s)/k_s$ is determined. In other words, for each given aggregate k_0, the saturation degree at stable state $(k_{max} - k_s)/k_s$ is dependent on $\mu\dot{\gamma}$. As for the fluid shear stress condition $\mu\dot{\gamma}$, it is rescaled with the strength of aggregate at limit structure, i.e. $\mu\dot{\gamma}/(\sigma_0 k_{max}\phi_{max})$. Physical image of such scaling can be understood as following: instead of applying
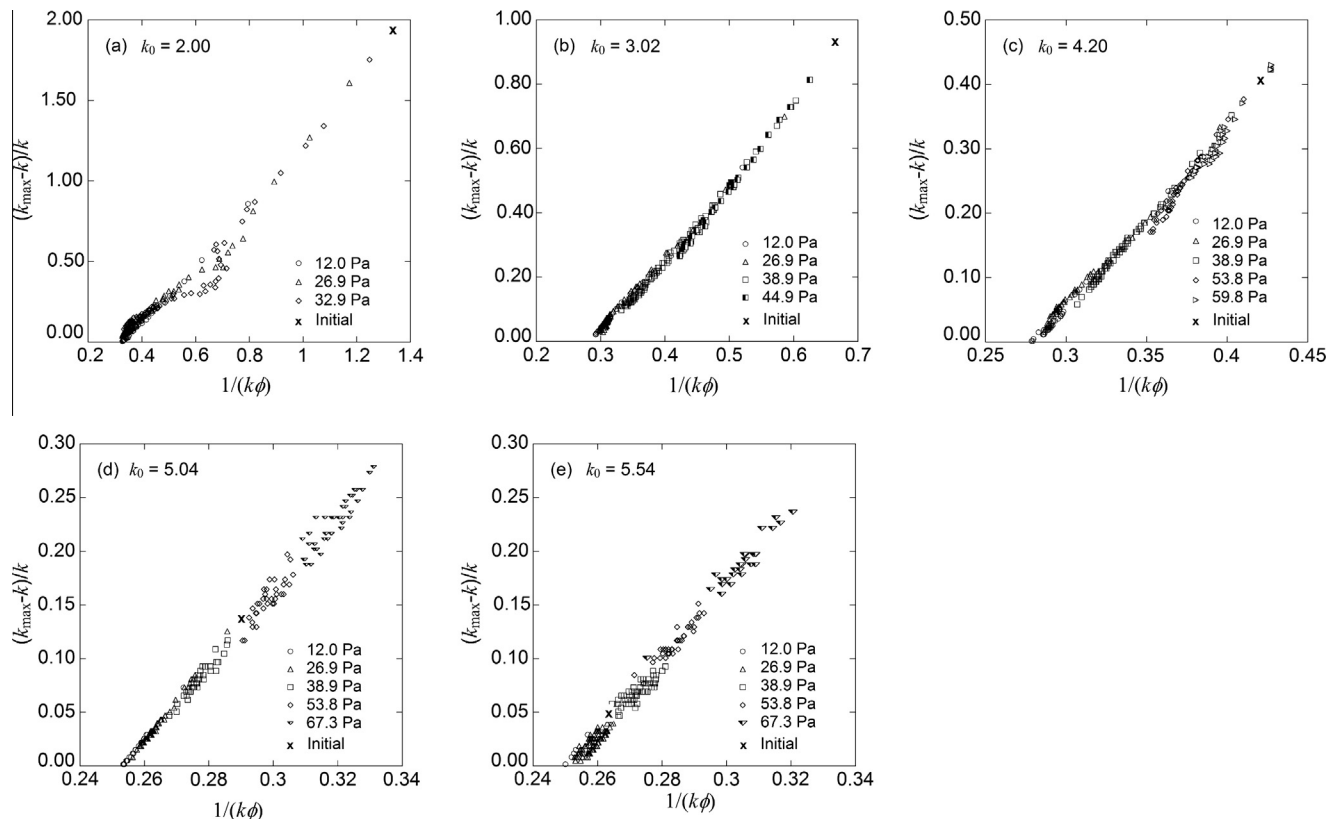

Fig. 5. Relation of the saturation degree $(k_{max} - k)/k$ and inversed strength of aggregate $1/(k\phi)$ during the restructuring form initial structure toward stable structure in various shear conditions.

$\mu\dot{\gamma}$ directly to the initial aggregate, the aggregate is firstly put in weak flow condition so that a limit structure is achieved, then the weak flow is switched to $\mu\dot{\gamma}$. As a result, $\mu\dot{\gamma}/(\sigma_0 k_{\max}\phi_{\max})$ inherently indicates the restructuring of the limit aggregate $k_{\max}$ under the fluid flow $\mu\dot{\gamma}$, rather than that of k_0. Readers may refer to Fig. 3 for a clearer illustration. Fig. 6 expresses the relation of $(k_{\max} - k_s)/k_s$ and $\mu\dot{\gamma}/(\sigma_0 k_{\max}\phi_{\max})$ for many aggregates. It reveals that when the fluid shear stress is normalized by the strength of the limit aggregate, the saturation degree $(k_{\max} - k_s)/k_s$ becomes independent of the initial structure. Fig. 6 also shows that $(k_{\max} - k_s)/k_s$ increases with $\mu\dot{\gamma}/(\sigma_0 k_{\max}\phi_{\max})$, meaning that if shear flow is strong, the aggregate is more loose and weaker compared to the limit structure. In conclusion, with the assumption that the limit structure of the aggregate is valid for any aggregate, one can determine not only the properties of stable aggregate for any fluid condition (by Fig. 6), but also the change in the properties of aggregate toward stable state (by Fig. 5).

Furthermore, we find that the value of $(k_{\max} - k_s)/k_s$ in Fig. 6 also reveals relation to kinetics of restructuring. The proposed kinetic model of the restructuring and its verification can be found in the previous study [20]. The model describes the temporal change in coordination number during the restructuring. The core of the model is analogous to micromechanics of granular material. The change rate of coordination number $dk/d(\dot{\gamma}t)$ comprises of two parallel components: (i) forming rate which is proportional to the number of unlinked particles, i.e. the available space around particle, defined as $C^+(k_{\max} - k)$, and (ii) cut rate which is proportional to the number of linked particles, defined as $C^- k$. In the model, C^+ and C^- are proportional coefficients determined by least-square method from the simulation data. Fig. 7 shows the simulation result and the model result for aggregate $k_0 = 3.02$ at different $\mu\dot{\gamma}$. From the model, when the stable structure of aggregate is obtained, the formation rate and the cut rate of particle is equal, leading to $C^-/C^+ = (k_{\max} - k_s)/k_s$. This result reveals the relation of kinetic coefficients and the dynamic property of the aggregate. Fig. 6 which exhibits the saturation degree of stable aggregate $(k_{\max} - k_s)/k_s$ not only helps to predict the properties of stable aggregate in the corresponding fluid condition, but also directly provides information for the kinetics. In addition, the value of $(k_{\max} - k_s)/k_s$ in Fig. 6 can be classified into two parts: $(k_{\max} - k_s)/k_s \to 0$ and $(k_{max} - k_s)/k_s > 0$. When $\mu\dot{\gamma}/(\sigma_0 k_{\max}\phi_{\max}) \leqslant 2.3 \times 10^{-2}$, the saturation degree $(k_{\max} - k_s)/k_s \to 0$, or $C^-/C^+ \to 0$, which can be interpreted as $C^- \to 0$ while $C^+ \neq 0$. It means that when the aggregate restructure from k_0 to $k_{\max}$ in weak flow, the weak flow induces the connection of particles but is not strong enough to break the link once it is made. Then, after the limit aggregate $k_{\max}$ is obtained in weak flow, $C^-/C^+ \to 0$ reveals that
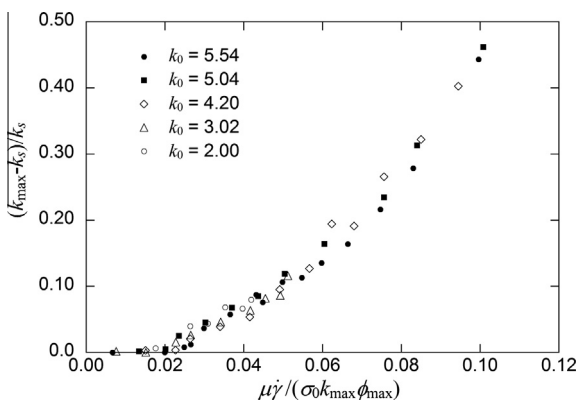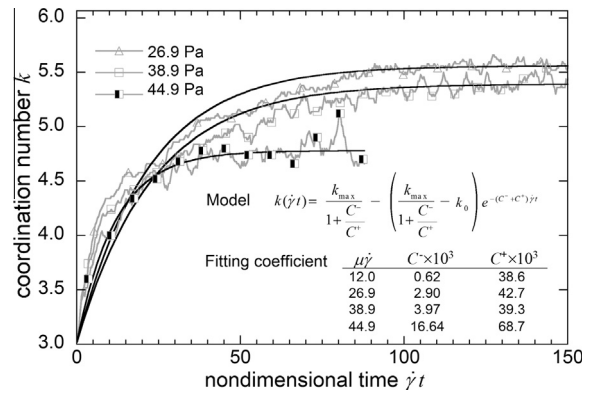

Fig. 7. Change in coordination number with nondimensional time by simulation results and model results for the initial aggregate of $k_0 = 3.02$ at different fluid shear rate.

the flow has no effect on aggregate except for the rotation. Otherwise, when the flow is strong enough $\mu\dot{\gamma}/(\sigma_0 k_{\max}\phi_{\max}) > 2.3 \times 10^{-2}$, then $C^-/C^+ > 0$, and the new stable structure is in dynamic equilibrium. We can further confirm this conclusion by Fig. 3: in weak flow condition ($\mu\dot{\gamma} = 12.0$ Pa), the temporal change after obtaining $k_{\max}$ is smooth with almost no fluctuation, whereas in stronger flow $\mu\dot{\gamma} \geqslant 26.9$ Pa, the profile after obtaining k_s has small periodic fluctuation. Such periodic fluctuation indicates the dynamic equilibrium for $C^-/C^+ > 0$.

3.3. Factors affecting the restructuring behavior of aggregate

As mentioned elsewhere, the hydrodynamic stress acting on aggregate and the cohesive strength of the aggregate play a crucial role for understanding the behavior of aggregate in fluid flow. Compared to the breakup event which is fast and instant, the restructuring is much more complex because it takes place continuously, leading to successive changes in the resulting hydrodynamic stress acting on aggregate and the strength of aggregate. In this section, we examine the exact contribution of these two parameters on the restructuring of non-fractal aggregate.
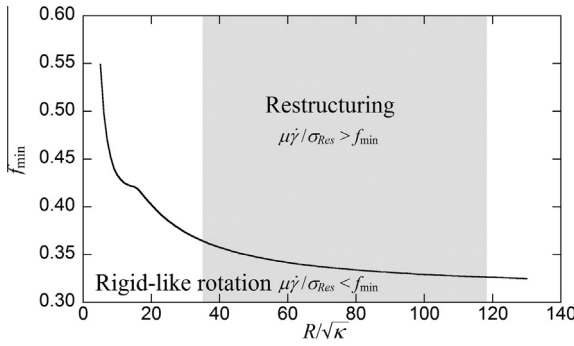
We analyze the aggregate in a similar manner with the analytical method for predicting the breakup of aggregate proposed by Adler and Mills [34]. They consider that aggregate is a uniformly porous sphere, the breakup of aggregate is fast, and deformation of aggregate is negligibly small. The hydrodynamics inside and outside the sphere is governed by continuity, Stokes equation and Brinkman equation. The velocity field induces effect on the internal stress of the porous sphere. Because the porous medium does not deform, the relation of velocity field and the solid stress tensor $\boldsymbol{\sigma}$ of the porous sphere can be analytically obtained. Then the breakup of the porous sphere is predicted by the solid stress tensor $\boldsymbol{\sigma}$ and the strength of the porous medium S. As the Mises yield condition is applied, the criterion for the sphere not to breakup is defined as Eq. (7).

$$\boldsymbol{\sigma}_D : \boldsymbol{\sigma}_D \leqslant 2S^2 \tag{7}$$

where $\boldsymbol{\sigma}_D$ is the deviatoric part of the solid stress tensor $\boldsymbol{\sigma}$. In the case of simple shear flow, the equivalent form of Eq. (7) can be rewritten as

$$\left(\frac{\mu\dot{\gamma}}{S}\right)_{Break} \leqslant f_{min}(R, \kappa, p, \boldsymbol{r}) \tag{8}$$

In Eq. (8) above, f depends only on the properties of the porous sphere, including the radius R of the sphere, the permeability κ, Poisson ratio p of the porous medium, and the position $\boldsymbol{r}$ inside

Fig. 6. Relation of stable structure of aggregate with fluid shear stress $\mu\dot{\gamma}$ and the limit structure $k_{\max}\phi_{\max}$.

Fig. 8. Restructuring regime of aggregate as a function of screened radius of aggregate. f_{min} is determined by porous sphere model [34]. The gray area shows the restructuring regime for the investigated conditions in this study.

the sphere. For a given porous sphere, f varies with the position $\boldsymbol{r}$ inside the sphere. Choosing the position $\boldsymbol{r}$ to minimize f is required for the use of the breakup criterion in Eq. (8). Details of the calculation are given in Appendix A.2. The function $f(R, \kappa, p, \boldsymbol{r})$ can be roughly interpreted as the penetration effect of flow field on the resulting stress acting on the porous sphere. The above relation means that for a porous sphere whose properties are known, a critical fluid shear stress for the breakup can be specified. The breakup event in the model is assumed instant, i.e., parts of sphere detach without changing their structure.

In our study, we have shown that at weak flow condition the aggregate exist in the form of limit structures (shown by the constant region k_{max} of Fig. 2, or $(k_{max} - k_s)/k_s \approx 0$ region in Fig. 6). Such limit aggregate are spherical, and rotate like a rigid body, therefore it is suitable to consider the aggregate as a porous sphere. If the flow is stronger, the aggregate restructures from the limit structure toward another one whose connectivity is less connected than k_{max}. Differ from Adler and Mills [34] where the criterion is used between the rigid-like behavior and breakup, here we apply the model for the rigid-like behavior and restructuring. The criterion is similar to Eq. (8) and given as

$$\frac{\mu\dot{\gamma}}{\sigma_{Res}} \leqslant f_{min}(R, \kappa, p, \boldsymbol{r}) \tag{9}$$

where σ_{Res} is characteristic restructuring strength of aggregate, the value of f_{min} shows the influence of aggregate properties, e.g. size, permeability, on the resulting hydrodynamic stress acting on the aggregate as mentioned above. We assume that the limit aggregate is a porous sphere whose permeability is based on Happel's formula [35]:

$$\kappa = \frac{2}{9}\frac{a^2}{\phi}\frac{3 - \frac{9}{2}\phi^{\frac{1}{3}} + \frac{9}{2}\phi^{\frac{5}{3}} - 3\phi^2}{3 + 2\phi^{\frac{5}{3}}} \tag{10}$$

In Eq. (10), a is the radius of particle, ϕ is the volume fraction of aggregate. Then f_{min} is numerically calculated for various values of $R/\sqrt{\kappa}$ which physically represent the screened radius of the

aggregate or, in other words, the size of aggregate compared to the size of the pore (Appendix A.2). Fig. 8 shows the dependence of f_{min} on $R/\sqrt{\kappa}$ for $p = 0$. We find out that there is no significant difference for $0 \leqslant p \leqslant 0.25$. In general, the decrease in f_{min} with $R/\sqrt{\kappa}$ means that the fluid flow is more difficult to penetrates the more dense aggregate. As a result, the resulting hydrodynamic stress acting on the dense aggregate is higher than that on loose aggregate. Moreover, according to Eq. (9), two regions are determined in Fig. 8: below and above the curve. The region below the curve indicates the conditions that when the applied fluid shear stress $\mu\dot{\gamma}$ and the restructuring strength of aggregate σ_{Res} satisfy $\mu\dot{\gamma}/\sigma_{Res} \leqslant f_{min}$, the aggregate behaves like a rigid body. The region above the curve denotes the case $\mu\dot{\gamma}/\sigma_{Res} > f_{min}$ where the aggregate restructures. As for the investigated condition in this study, the restructuring regime falls in the gray area. Table 3 provides the data for the initial aggregate and the limit aggregate obtained in weak flow $\mu\dot{\gamma} = 12.0$ Pa. In this gray part, f_{min} does not significantly vary, i.e., the effect of penetration of fluid flow on the resulted hydrodynamic stress acting on the aggregate plays a minor role. It means that when construct a model describing the restructuring of non-fractal aggregate based on the hydrodynamic stress and strength of aggregate, the parameter describing the influence of structure on hydrodynamic stress can be simplified even for the case of the very loose aggregate. Therefore, model should focus on the effect of the strength of aggregate. Also in the simulation of hydrodynamic force on the particles of non-fractal aggregate, the screening effect of the outer particles to the inner ones should be considered, for example, the use of free draining approximation in such case may overestimate the effect of fluid flow. Relating to the criterion, it is worth to note that the strength of porous media S in breakup criterion by Adler and Mills is a known parameter [34], whereas the characteristic restructuring strength σ_{Res} in restructuring criterion Eq. (9) is unknown. We combine the porous sphere model and our simulation results to determine restructuring strength σ_{Res}. We assume that the restructuring strength is proportional to tensile strength of aggregate $\sigma_{Res} = \alpha\sigma_{Rumpf}$, then the ratio of restructuring strength to tensile strength, is determined in the range of $\alpha \approx 1/14$–$1/20$ (Table 3). It is reasonable when the restructuring strength is smaller than the tensile strength [16]. The result can be used for developing a restructuring model for non-fractal aggregate.

4. Conclusion

The restructuring behavior of non-fractal aggregate in simple shear flow has been numerically investigated. The many-particle hydrodynamic interaction is estimated by Stokesian dynamics while the interparticle interaction is calculate from van der Waals potential. During the restructuring, the connectivity of the particles of the aggregate has changed toward a stable structure depending on the shear condition. The dependence of coordination number and volume fraction of aggregate on flow condition and nondimensional time is very complex. A linear relation of the saturation

Table 3
Properties of initial aggregate and limit aggregate obtained at weak flow condition using porous sphere model. The assumed Poisson ratio is $p = 0$, the value of $\mu\dot{\gamma}^*$ is determined from Fig. 2.

Initial structure						Limit structure at weak flow condition							
k_0	ϕ_0	R_0/a	$\kappa_0/a^2 \times 10^3$	$R_0/\sqrt{\kappa_0}$	f_{min}	$\mu\dot{\gamma}^*$	k_{max}	ϕ_{max}	R/a	$\kappa/a^2 \times 10^3$	$R/\sqrt{\kappa}$	f_{min}	$1/\alpha$
2.00	0.371	6.46	38.2	33.1	0.368	12	5.92	0.516	5.79	10.1	57.7	0.343	19.4
3.02	0.488	5.90	13.1	51.5	0.347	16	5.96	0.596	5.52	4.54	81.9	0.334	16.4
4.20	0.559	5.63	6.62	69.2	0.338	16	5.92	0.602	5.50	4.26	84.2	0.333	16.5
5.04	0.654	5.35	2.40	109.1	0.328	20	6.09	0.658	5.34	2.30	111.4	0.328	14.6
5.54	0.665	5.32	2.11	115.7	0.327	20	6.10	0.666	5.32	2.09	116.3	0.327	14.8

degree of particle connection, and the inversed strength of aggregate during restructuring is recognized. We have found the limit of restructuring: under weak flow, the aggregate obtains its most compact structure whose properties can be typically determined. Such limit aggregates play important role for the prediction of restructuring behavior.

Appendix A

A.1. Calculation of volume fraction of aggregate

The aggregate is considered to be equivalent of an ellipsoid which has the same principal of moment of inertia [31]. The inertia tensor $\boldsymbol{I}$ of the aggregate is calculated as follows

$$
\boldsymbol{I} = \begin{bmatrix} \sum_{i=1}^{N}\left[(y_i - y_c)^2 + (z_i - z_c)^2\right] & -\sum_{i=1}^{N}(x_i - x_c)(y_i - y_c) & -\sum_{i=1}^{N}(x_i - x_c)(z_i - z_c) \\ -\sum_{i=1}^{N}(x_i - x_c)(y_i - y_c) & \sum_{i=1}^{N}\left[(x_i - x_c)^2 + (z_i - z_c)^2\right] & -\sum_{i=1}^{N}(y_i - y_c)(z_i - z_c) \\ -\sum_{i=1}^{N}(x_i - x_c)(z_i - z_c) & -\sum_{i=1}^{N}(y_i - y_c)(z_i - z_c) & \sum_{i=1}^{N}\left[(x_i - x_c)^2 + (y_i - y_c)^2\right] \end{bmatrix}
$$

where x_c, y_c, z_c are the coordinates of the center of mass of aggregate composed of N particle, x_i, y_i, z_i the coordinates of the ith particle in the aggregate. The eigenvalues I_1, I_2, I_3 of the eigenvectors determined from the inertia tensor $\boldsymbol{I}$ are the three principal moment of inertia. The length of the semi-principal axis of the equivalent ellipsoid is given by the followed equations.

$$
a_1 = \sqrt{\frac{5}{2}\frac{I_2 + I_3 - I_1}{N}}, \quad a_2 = \sqrt{\frac{5}{2}\frac{I_1 + I_3 - I_2}{N}}, \quad a_3 = \sqrt{\frac{5}{2}\frac{I_1 + I_2 - I_3}{N}}
$$

The volume fraction of the aggregate, which is the ratio of the total volume of particles to the volume of the equivalent ellipsoid, is straightforwardly given as

$$
\phi = \frac{N}{a_1 a_2 a_3}
$$

A.2. Calculation of the value f by the porous sphere model [34]

The porous sphere model proposed by Adler and Mills [34] is able to calculate the hydrodynamic stress acting on a position inside the non-deformable porous sphere. The calculation is performed in spherical coordinates for an arbitrary position $\boldsymbol{r}(r, \theta, \phi)$ inside the porous sphere of radius R. The nondimensional radius is employed, defined as $\xi = \frac{r}{\sqrt{\kappa}}$ and $\xi_1 = \frac{R}{\sqrt{\kappa}}$. The value of the right hand side of Eq. (9) is calculated as following

$$
f = \frac{\sqrt{2}}{5}\frac{10\hat{\psi}_2 + \hat{\psi}_0}{\sqrt{A}}
$$

The ξ-dependent function ψ_n and the ξ_1-dependent function $\hat{\psi}_n$ are denoted as

$$
\psi_n = \psi_n(\xi) = \left(\frac{1}{\xi}\cdot\frac{d}{d\xi}\right)^n \frac{sinh\xi}{\xi}
$$

$$
\hat{\psi}_n = \psi_n(\xi_1)
$$

The value of A is determined as follows

$$
\begin{aligned}
A = {} & 2\left[I + \frac{1}{2}U\hat{\psi}_2(\xi_1^2 - 3\xi^2) - F\hat{\psi}_2\right]^2 + \xi^2\sin^2\theta\left[J\left(\frac{J}{2} + \frac{2I}{\xi}\right)\right. \\
& + U\hat{\psi}_2\left(4I + J\frac{\xi_1^2 - \xi^2}{\xi}\right) + 2U^2\hat{\psi}_2(\xi_1^2 - 2\xi^2) - 4F\hat{\psi}_2\left(\frac{J}{2\xi} + U\hat{\psi}_2\right)\right] \\
& + 4\xi^4\sin^4\theta\cos^2\varphi\sin^2\varphi \times \left\{(\psi_2 - 7\psi_3)^2 + \psi_3^2 + \frac{K^2}{2\xi^2}\right. \\
& \left. - \psi_4(2I + J\xi + K\xi) + U\hat{\psi}_2[2\psi_3 - 4\psi_4 U\hat{\psi}_2(\xi_1^2 - \xi^2)] + \frac{2}{3}U_2\hat{\psi}_2^2 + 2\psi_4 F\hat{\psi}\right\}
\end{aligned}
$$

The function I, J, K in the above equation is dependent on ξ and ξ_1

$$
I = 2\hat{\psi}_2 - 2\psi_2 + \psi_1, \quad J = \xi(\psi_2 - 4\psi_3), \quad K = \xi(\psi_2 - 6\psi_3)
$$

The parameters b, U, V and W express the property of the porous sphere via the screened radius ξ_1 and the Poisson's ratio p, denoted as

$$
b = 1 - 8\frac{\hat{\psi}_3}{\hat{\psi}_2}, \quad U = \frac{1 + p - 3bp}{7 + 5p},
$$

$$
V = \frac{4 + 2p - b(7 - 4p)}{2(7 + 5p)},
$$

$$
W = \frac{6 + 4p - b(7 + 2p)}{2(7 + 5p)} - \frac{1}{\xi_1^2}\cdot\frac{5\hat{\psi}_1 - \hat{\psi}_0 - 20\hat{\psi}_2}{2\hat{\psi}_2}
$$

Finally, F is defined as

$$
F = \xi_1^2\left(W + \frac{U}{2}\right) - \xi^2\left(\frac{3U}{2} + V\right)
$$

In general, for a given porous sphere whose properties are fixed, the value of f is only dependent on the position of the porous sphere. The extremes of f are numerically obtained by searching thorough the porous sphere.

References

[1] Y.M. Harshe, M. Lattuada, M. Soos, Experimental and modeling study of breakage and restructuring of open and dense colloidal aggregates, Langmuir 27 (2011) 5739–5752.
[2] S.P. Rwei, I. Manas-Zloczower, D.L. Feke, Observation of carbon black agglomerate dispersion in simple shear flow, Polym. Eng. Sci. 30 (1990) 701–706.
[3] S. Blaser, Flocs in shear and strain flows, J. Colloid Interface Sci. 225 (2000) 273–284.
[4] S. Harada, R. Tanaka, H. Nogami, M. Sawada, Dependence of fragmentation behavior of colloidal aggregates on their fractal structure, J. Colloid Interface Sci. 301 (2006) 123–129.

[5] V. Becker, E. Schlauch, M. Behr, H. Briesen, Restructuring of colloidal aggregates in shear flows and limitations of the free-draining approximation, J. Colloid Interface Sci. 339 (2009) 362–372.

[6] M.L. Eggersdorfer, D. Kadau, H.J. Herrmann, S.E. Pratsinis, Fragmentation and restructuring of soft-agglomerates under shear, J. Colloid Interface Sci. 342 (2010) 261–268.

[7] S. Horwatt, I. Manas-Zloczower, D.L. Feke, Dispersion behavior of heterogeneous agglomerates at supercritical stresses, Chem. Eng. Sci. 47 (1992) 1849–1855.

[8] K. Higashitani, K. Iimura, H. Sanda, Simulation of deformation and breakup of large aggregates in flows of viscous fluids, Chem. Eng. Sci. 56 (2001) 2927–2938.

[9] A. Kimbonngfuila Manounou, S. Rémond, Discrete element modeling of the microstructure of fine particle agglomerates in sheared diluted suspension, Physics A 412 (2014) 66–83.

[10] C. Selomulya, G. Bushell, R. Amal, T.D. Waite, Understanding the role of restructuring in flocculation: the application of a population balance model, Chem. Eng. Sci. 58 (2003) 327–338.

[11] L. Gmachowski, Aggregate restructuring and its effect on the aggregate size distribution, Colloids Surf. A: Physicochem. Eng. Aspects 207 (2002) 271–277.

[12] S. Markutsya, R.O. Fox, S. Subramaniam, Characterization of sheared colloidal aggregateion using Langevin dynamics simulation, Phys. Rev. E 89 (2014) 062312.

[13] B.O. Conchuir, Y.M. Harshe, M. Lattuada, A. Zaccone, Analytical model of fractal aggregate stability and restructuring in shear flows, Ind. Eng. Chem. Res. 53 (2014) 9109–9119.

[14] R. Seto, R. Botet, G.K. Auernhammer, H. Briesen, Restructuring of colloidal aggregates in shear flow: coupling interparticle contact models with Stokesian dynamics, Eur. Phys. J. E 35 (2012) 128–139.

[15] A. Zaccone, M. Soos, M. Lattuada, H. Wu, M.U. Bäbler, M. Morbidelli, Breakup of dense colloidal aggregates under hydrodynamic stresses, Phys. Rev. E 79 (2009) 061401.

[16] M. Vanni, A. Gastaldi, Hydrodynamic forces and critical stresses in low-density aggregates under shear flow, Langmuir 27 (2011) 12822–12833.

[17] S. Harada, R. Tanaka, H. Nogami, M. Sawada, K. Asakura, Structural change in non-fractal particle clusters under fluid stress, Colloids Surf. A: Physicochem. Eng. Aspects 302 (2007) 396–402.

[18] K. Horii, R. Yamada, S. Harada, Strength deterioration of nonfractal particle aggregates in simple shear flow, Langmuir 31 (2015) 7909–7918.

[19] N.D. Vassileva, D. van den Ende, F. Mugele, J. Mellema, Restructuring and break-up of two-dimensional aggregates in shear flow, Langmuir 22 (2006) 4959–4967.

[20] U.T. Lieu, S. Harada, Stability of restructured non-fractal aggregates in simple shear flow, Adv. Powder Technol. 26 (2015) 705–710.

[21] J.F. Brady, G. Bossis, Stokesian dynamics, Ann. Rev. Fluid Mech. 20 (1988) 111–157.

[22] L. Durlofsky, J.F. Brady, G. Bossis, Dynamic simulation of hydrodynamically interacting particles, J. Fluid Mech. 180 (1987) 21–49.

[23] D.J. Jeffery, Y. Onishi, Calculation of the resistance and mobility functions for two unequal rigid spheres in low-Reynolds-number flow, J. Fluid Mech. 139 (1984) 261–290.

[24] S. Kim, S.J. Karrila, Microhydrodynamics, Butterworth-Heinemann, Boston, 1991.

[25] H.C. Hamaker, The London-van der Waals attraction between spherical particles, Physica 4 (1937) 1058–1072.

[26] W.R. Bowen, F. Jenner, The calculation of dispersion forces for engineering application, Colloid Interface Sci. 56 (1995) 201–243.

[27] J.N. Israelachvili, Intermolecular and Surface Force, Academic Press, London, 1992.

[28] J.P. Pantina, E.M. Furst, Elasticity and critical bending moment of model colloidal aggregates, Phys. Rev. Lett. 94 (2005) 138301.

[29] Y.M. Harshe, M. Lattuada, Breakage rate and colloidal aggregates in shear flow through Stokesian dynamics, Langmuir 28 (2012) 283–292.

[30] L.F. Liu, Z.P. Zhang, A.B. Yu, Dynamic simulation of the centripetal packing of mono sized spheres, Physics A 268 (1999) 433–453.

[31] Y.M. Harshe, L. Ehrl, M. Lattuada, Hydrodynamic properties of rigid fractal aggregates of arbitrary morphology, J. Colloid Interface Sci. 352 (2010) 87–98.

[32] A. Kansal, S. Torquato, F.H. Stillinger, Diversity of order and densities in jammed hard-particle packings, Phys. Rev. E 66 (2002) 041109.

[33] H. Rumpf, Zur Theorie der Zugfestigkeit von Agglomeraten bei Kraftubertragung an Kontaktpunkten, Chem. Ing. Tech. 42–8 (1970) 538–540.

[34] P.M. Adler, P.M. Mills, Motion and rupture of a porous sphere in a linear flow field, J. Rheol. 23–1 (1979) 25–37.

[35] J. Happel, Viscous flow in multiparticle systems: slow motion of fluids relative to beds of spherical particles, AIChE J. 4 (1958) 197–201.